J. Am. Soc. Mass Spectrom. (2015) 26:958–966
DOI: 10.1007/s13361-015-1128-8

FOCUS: IMAGING MASS SPECTROMETRY : RESEARCH ARTICLE

Mass Spectrometry Imaging and GC-MS Profiling of the Mammalian Peripheral Sensory-Motor Circuit

Stanislav S. Rubakhin,[1] Alexander Ulanov,[2] Jonathan V. Sweedler[1]

[1]Department of Chemistry, University of Illinois at Urbana-Champaign and the Beckman Institute for Advanced Science and Technology, Urbana, IL 61801, USA
[2]Roy J. Carver Biotechnology Center, University of Illinois at Urbana-Champaign, Urbana, IL 61801, USA

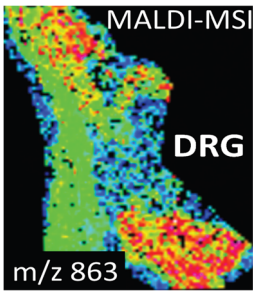

Abstract. Matrix-assisted laser desorption/ionization (MALDI) mass spectrometry imaging (MSI) has evolved to become an effective discovery tool in science and clinical diagnostics. Here, chemical imaging approaches are applied to well-defined regions of the mammalian peripheral sensory-motor system, including the dorsal root ganglia (DRG) and adjacent nerves. By combining several MSI approaches, analyte coverage is increased and 195 distinct molecular features are observed. Principal component analysis suggests three chemically different regions within the sensory-motor system, with the DRG and adjacent nerve regions being the most distinct. Investigation of these regions using gas chromatography-mass spectrometry corroborate these findings and reveal important metabolic markers related to the observed differences. The heterogeneity of the structurally, physiologically, and functionally connected regions demonstrates the intricate chemical and spatial regulation of their chemical composition.

Keywords: Mass spectrometry imaging, Gas chromatography-mass spectrometry, Peripheral sensory-motor system, Dorsal root ganglia, Spinal nerve

Received: 6 February 2015/Revised: 3 March 2015/Accepted: 3 March 2015/Published Online: 31 March 2015

Introduction

The spatial-temporal chemical and structural heterogeneity of the nervous system is enormous, making the evaluation of the tissue or organ metabolome at spatial resolutions approaching the single cell level problematic as the metabolome varies in a region and cell-specific manner. Mass spectrometry imaging (MSI) is a multifaceted analytical approach that allows the spatial localization and characterization of a broad range of analytes at the tissue, cellular, and even subcellular levels [1–7]. Caprioli has played a pivotal role in the introduction, development, and popularization of matrix-assisted laser desorption/ionization (MALDI)-MSI [4, 5, 8–10]. The approach typically delivers multiplexed information, with tens to hundreds of compounds detected at each location within a sample. Because of the chemical complexity of tissues, this analyte coverage is not enough to characterize the complete metabolome, peptidome, or proteome. Although a range of additional analyte separation and conditioning steps have been developed, they are not easily implemented because of the thousands of individual spots sampled across a sample surface during MSI.

To address the problem of low analyte coverage, several off-line and on-line strategies have been implemented, including pre-separation of ions using ion mobility approaches [11–14], high resolution mass analyzers [8, 15–18], and liquid chromatography pre-separation of analytes [9]. One of the more obvious strategies to increase analyte coverage is to combine several MSI methods, each optimized for specific analyte classes [19–22]. For example, MALDI-MSI uses a variety of matrices that preferentially enhance the desorption/ionization of specific classes of analytes [23]. At times, the presence of MALDI matrix complicates the detection of metabolites because matrix ions may dominate the mass spectra and/or overlap with endogenous signals. An older approach, laser desorption/ionization (LDI), can be successfully used for some analytes while generating less background ions. As MALDI-MSI and LDI-MSI are performed on the same instrument, combining the two is a straightforward methodology to implement in discovery experiments. Of course, because this combination increases

Electronic supplementary material The online version of this article (doi:10.1007/s13361-015-1128-8) contains supplementary material, which is available to authorized users.

Correspondence to: Jonathan Sweedler; *e-mail:* jsweedle@illinois.edu

the time required to probe samples, smaller specimens of many brain regions or endocrine structures such as the pituitary [24–26] and spinal cord [27–31] are best suited to this strategy.

For this work, we performed MSI and other investigations of several areas of the mammalian sensory-motor system comprising the well-defined and compact dorsal root ganglion (DRG) and adjacent nerves (dorsal root, ventral root, and spinal nerve) in order to determine how the chemistry of different regions correlates to known structural motifs. A variety of animal nerves have been investigated by direct and indirect MS approaches, including the stomatogastric nerve of the blue crab *Callinectes sapidus* [32], the major connectives in the mollusk *Aplysia californica* [33], the mouse sciatic nerve [34], the rodent optic nerve [35], and the rat tibial [36] and lumbar nerves [37].

The DRG is a morphologically and biochemically complex structure containing thousands of cells having various functions, including proprioception and nociception. The DRG is a well-established neurobiological model that is widely-used in investigations of the mammalian nervous system's normal and pathologic activities [36, 38–41]. There are more than 5000 papers that describe different aspects of DRG morphology, physiology, and biochemistry, including MS-based studies of their elemental [42], metabolite [36, 43–45], and protein [46–49] contents. Axons of most DRG-located neurons are bifurcated, with the resulting branches extending inside the nerves towards the periphery (e.g., skin) and spinal cord. The nerves are complex structures where many neurites are ensheathed by Schwann cells and grouped in bundles surrounded by the epineurium and the perineurium. The presence of high lipid content in the myelin sheath makes these nerves difficult targets for direct MS investigation of endogenous peptides and proteins. However, the important role of nerves in normal and pathologic peripheral information collection and centrally generated signal conduction make them important targets for metabolomic [36, 43, 44] and proteomic [46] studies. In this work, after optimization of tissue sampling protocols, both LDI-MSI and MALDI-MSI were utilized to investigate the chemical heterogeneity of the functionally connected regions of the mammalian peripheral sensory-motor network.

Experimental

Chemicals

All reagents were purchased from Sigma-Aldrich (St. Louis, MO, USA) unless otherwise specified.

Biological Samples

All procedures related to animal handling and euthanasia were performed in accordance with local, state, and federal regulations and approved by the Illinois Institutional Animal Care and Use Committee. DRGs, spinal and sciatic nerves, and ventral and dorsal roots were surgically dissected from adult 6–12 wk-old Long-Evans/BluGill male and female rats (University of Illinois at Urbana-Champaign), euthanized by decapitation. To reduce the detrimental metabolic effects of a stopped blood flow, 40–60 mL of ice-cold Gey's balanced salt solution (mGBSS) was injected under the skin above the location of the DRGs of interest (the lumbar area) immediately after decapitation. The spinal canal was surgically opened, the spinal cord removed, and DRGs with adjacent nerves were individually isolated and placed into ice-cold mGBSS containing (in mM): 1.5 $CaCl_2$, 4.9 KCl, 0.2 KH_2PO_4, 11 $MgCl_2$, 0.3 $MgSO_4$, 138 NaCl, 27.7 $NaHCO_3$, 0.8 Na_2HPO_4, and 25 HEPES, pH 7.2. In gas chromatography-mass spectrometry (GC-MS) experiments, a mixture of 33% (v/v) glycerol and 67% mGBSS was used to stabilize the chemistry of the studied system after isolation.

MSI

MSI was performed on sections of the DRG and adjacent nerves. The DRGs and nerves were frozen and sectioned in 10-µm-thick slices without chemical fixation at –20°C using a Leica CM 3050 S cryostat (Leica Microsystems, Bannockburn, IL, USA). DRG sections were deposited on room temperature (23–25°C) indium tin oxide coated (ITO) glass slides (Bruker Daltonics, Billerica, MA, USA) and dried in a desiccator at 23–25°C for LDI-MSI. Specimens for MALDI-MSI were spray coated with 5 mg/mL 2-(4-hydroxyphenylazo) benzoic acid (HABA) in methanol/water-containing a 0.1% formic acid and 0.01% trifluoroacetic acid (TFA) (20/80 v/v) mixture or with 10 mg/mL 9-aminoacridine (9-AA) in a water/ethanol/TFA (30/70/1, v/v/v) solution [50]. An artist's airbrush attached to an in-house nitrogen line was used to apply MALD I matrix solutions onto tissue slices. Depending on the composition of the MALDI matrix, the applications were performed from a 50 to 100 cm distance in several iterations, allowing formation of a thin layer of liquid on top of the slides and their complete drying. Application of MALDI matrix solution was stopped when a thin uniform layer of matrix formed on top of the tissue sections. The quality of coating was visually observed using a Leica MZ 7.5 high-performance stereomicroscope with a 7.9:1 zoom (Leica Microsystems Inc.).

MSI was performed with an Ultraflex II TOF-TOF mass spectrometer (Bruker Daltonics) operating in reflector mode at positive or negative polarities. The laser beam was set to "small", corresponding to a 2020–4040 µm diameter footprint. The acquired chemical images have either a 25 or 50 µm spatial resolution. Mass spectra were acquired over the *m/z* 20–2000 mass range. Mass spectrometer calibration was performed using a Peptide Calibration Standard Kit II (angiotensin II, angiotensin I, Substance P, bombesin, ACTH clip 1-17, ACTH clip 18-39, somatostatin 28, bradykinin fragment 1-7, renin substrate tetradecapeptide porcine) obtained from Bruker Daltonics. The standards were deposited onto ITO slide locations nearby the DRG sections. The peptide ions, and in some cases known endogenous ions, such as several of the most common lipids as well as MALDI-matrix ions, were used in the post-processing step for data recalibration. The following

were typical performance parameters for representative spots: mass resolution was typically between 1000 and 2500, and the mass error, which depended on location and topology of the sample, ranged between 30 and 120 ppm.

Integrated software was used for MSI data acquisition and processing: FlexControl 3 – control of the instrument and mass spectra acquisition; FlexImaging 3 and 4 – chemical image acquisition, visualization, and data processing; FlexAnalysis 3 – visualization and processing of individual mass spectra as well as batch data processing; and ClinProTools 3 – statistical analysis, including multivariate analysis of acquired data (all programs are from Bruker Daltonics).

GC-MS

L4 and L5 DRGs and adjacent nerves, as well as the distal portion of the sciatic nerve, were isolated from three animals during an ~1 h dissection procedure done on ice. The individual structures were placed in 200 μL of ice cold 33% glycerol, 67% mGBSS solution, and stored on ice. The DRGs and nerves were separated and individually weighed after Kimwipe-assisted removal of excess solution surrounding the tissues. The wet mass of the glycerinated tissues varied between less than 20 (DRGs) to several hundred (distal part of sciatic nerve) milligrams. Metabolite extraction was performed using a modified two-phase approach described in [51]. Briefly, 200 μL of a solution containing 2:1 (v/v) reagent grade methanol and chloroform, cooled to 4°C, was added to each tube. Tissues were homogenized on ice. Homogenates were centrifuged at 18,000*g* for 10 min at 4°C. Supernatant was collected and moved to fresh tubes and stored on ice. Chloroform (100 μL) was added to the remaining material (pellet). The pellets were homogenized on ice and 100 μL of water was added. Samples were briefly vortexed and centrifuged at 18,000*g* for 10 min at 4°C. Two phases were formed in the extract solution after the centrifugation: an upper phase containing methanol and water, and a lower phase containing chloroform. A glass syringe with a long fine needle (Hamilton, Reno, NV, USA) was used to collect the phases separately and place them into corresponding vials. The lower phase was combined with the supernatant collected during the first extraction and specified as the "L" sample. The upper phase was placed into fresh vials and specified as "T". All samples were dried in a SpeedVac concentrator (Thermo Scientific, San Jose, CA, USA).

Dried samples were derivatized according to Roessner et al. [52] with minor modifications: 90 min at 50°C with 80 μL of methoxyamine hydrochloride in pyridine (20 mg mL $^{-1}$) followed by 60 min treatment at 50°C with 80 μL*N*-Methyl-*N*-(trimethylsilyl)trifluoroacetamide (MSTFA). An internal standard (10 μL of C31 fatty acid) was added prior to trimethylsilylation.

A sample volume of 1 μL was injected onto the column with a split ratio of 5:1. The GC-MS system consisted of an Agilent 7890A (Agilent Technologies, Inc., Palo Alto, CA, USA) gas chromatograph, an Agilent 5975C mass selective detector, and an Agilent 7683B autosampler.

Gas chromatography was performed on a 60 m HP-5MS column with a 0.25 mm inner diameter and 0.25 μm film thickness (Agilent) with an injection temperature of 250°C, the interface set to 250°C, and the ion source adjusted to 230°C. The helium carrier gas was set at a constant flow rate of 1.5 ml min^{-1}. The temperature program was 5 min of isothermal heating at 70°C, followed by an oven temperature increase of 5°C min^{-1} to 310°C, and a final 20 min at 310°C. Mass spectra were recorded in the *m/z* 50–800 scanning range.

The spectra of chromatogram peaks were compared with the following electron ionization mass spectrum libraries: NIST08 [53], WILEY08 [54], and a custom library consisting of 1183 unique mass spectra for common, naturally occurring metabolites (their TMS derivatives, methyl esters, and some compounds that are not amenable to derivatization but also present in biological samples). Authentic standards were used in creation of the custom library. To allow comparison between samples, data were normalized to the internal standard (hentriacontanoic acid) in each chromatogram and fresh weight of each sample. The chromatograms and mass spectra were evaluated using the MSD ChemStation (Agilent) and AMDIS [53] programs. The retention time and mass spectra were implemented within the AMDIS method formats. Metabolite concentrations are reported as concentrations relative to the internal standard (i.e., target compound peak area divided by peak area of hentriacontanoic acid: $N_i = X_i \times X^{-1}$IS per 100 mg wet weight. The instrument variability was within the standard acceptance limit (5%). Three individual samples collected from three different animals were analyzed using GC-MS. GC-MS was performed in the Roy J. Carver Metabolomics Center at the University of Illinois at Urbana-Champaign.

Partial Least Squares-Discriminant Analysis (OPLS/O2PLS-DA) Model for Evaluation of GC-MS Results

For the metabolite profiling, the instrument variability was within the standard acceptance limit (5%). GC-MS analysis of both polar and nonpolar metabolites detected a total of ~1200 electron ionization mass spectral features in the samples. Of these, 194 compounds were positively identified, with the majority being lipids. Chemometric models were obtained using the SIMCA P+ (12.0) program (Umetrics, Umeå, Sweden). Metabolites with 80% or more missing data were removed from analysis; the rest of the missing values for particular metabolites were imputed with 0. All spurious metabolites derived from column bleed and reagent artifacts were also removed from the data sets.

Due to an uncertain principal component analysis (PCA) model, a supervised PLS analysis was performed on centered data for validation of the generated chemometric models. The number of observations used in chemometric models is typically much lower than the total number of variables; it is possible that the good performance statistics observed in the chemometric models could be due to data overfitting [55–57]. The obtained PLS-DA model was further analyzed using 7-fold

cross-validation ANOVA and response permutation with 900 random reclassifications (random assignment of class labels in order to test whether differences found between groups are significant). The observed PLS-DA model had R2Y = 16.9%, Q2 = –15.3% (negative prediction ability), and variables explained 81.1% (R2X) of total variation [55–61].

Results and Discussion

DRG Sample Preparation for MSI Analyses

The areas of the mammalian sensory-motor system under investigation here presented challenges for the MALDI-MSI and LDI-MSI analyses for two reasons. As highlighted in Figure 1, sample preparation necessitates repeatable longitudinal sectioning through sensory-motor areas, including long and thin nerves and small (~2–3 mm in diameter) DRGs. We developed an approach so that after surgical isolation, the structure was properly oriented and prepositioned on a piece of soft material (e.g., pack foam) cooled with an underlying layer of ice. In the next step, samples were stamped onto the surface, coated with ice, and cooled to –20°C in the cryostat's sample holder. The ice layer surface was pre-aligned with the cryostat's cutting knife before sample deposition, which allowed three to four 10-µm-thick sections to be cut through the entire central region of the DRG and associated nerves. The second challenge was the detection of different classes of analytes in nerves containing a large number of highly myelinated fibers possessing high concentrations of lipids. This issue was partially addressed by applying different ionization approaches as well as a range of MALDI matrices as described below.

MALDI-MSI of the Mammalian Sensory-Motor Network

MSI provides multiplexed, untargeted information on the chemical composition of the analyzed specimen. Our analysis of different regions of the mammalian peripheral sensory-motor system revealed surprising differences in the chemical profiles of the regions (Figure 2 and Supplementary Table S1), with each approach highlighting a different subset of compounds. Negative polarity LDI-MS generated the lowest number of ions, 30 (22 unique). The heaviest molecular ion detected was *m/z* 639.7, which could not be easily assigned to lipid signals previously observed in mammalian nervous system MSI experiments [62] (Supplementary Table S1). Positive polarity LDI-MS performed better, with 73 (54 unique) ions detected, including the highest molecular ion at *m/z* 1522.6. At least eight signals can be putatively assigned as lipids (Supplementary Table S1). The large number of ions in the *m/z* 600–900 mass range is common for molecular profiles of biological tissues studied with direct MS. LDI-MS profiles of different regions of the system were visually similar. Treatment of the samples with MALDI matrix increased the number of detected molecular features but also led to an increase in background ions. Thirty-four (24 unique) molecular ions were detected with negative mode MALDI-MS and 9-AA matrix. The largest *m/z* present in the mass spectra is 936.9. Twelve species can be putatively assigned as lipids (Supplementary Table S1). Predictably, positive mode MALDI-MS utilizing HABA as the matrix generated the largest quantity of both endogenous and background ions, with the number of background ions reaching 136, which is larger than the total number of biological sample-related molecular features, 119 (95 unique). Twenty-seven of the signals matched the *m/z* of expected lipids. Although the number of peaks can be improved by optimizing sample preparation, the data demonstrate the effectiveness of using a variety of MSI methods when analyte coverage is a concern.

Analysis of the spatiochemical MSI data reveals unique chemical profiles, call them regional biomarkers, for all of the distinct areas we studied (Figure 3). As examples, analytes with *m/z* 865 are predominantly present in nerves and roots but not in the DRG (the analyte may be associated with myelin); another signal with *m/z* 727 is

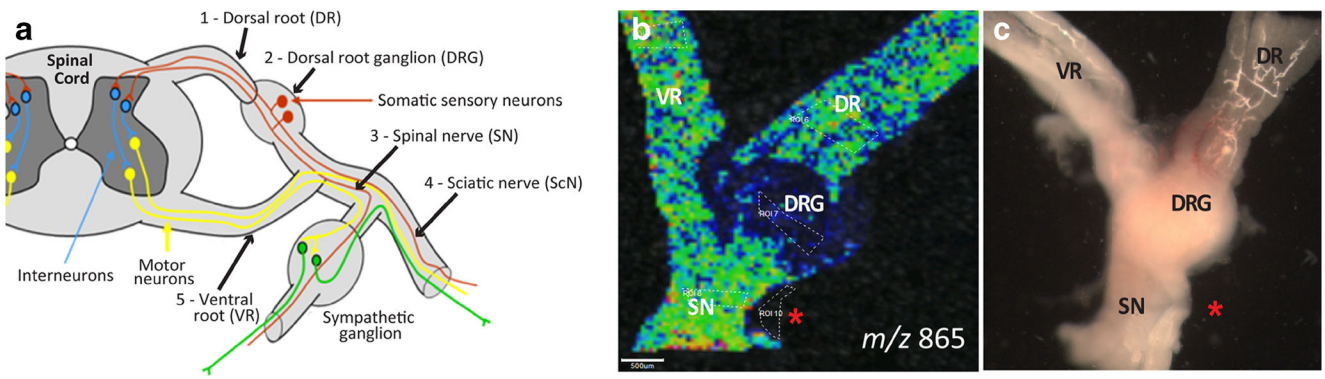

Figure 1. Dorsal root ganglia and adjacent nerves are located in close proximity to the spinal cord and contain satellite cells, sensory neurons and their neurites, neurites of motor neurons, along with glia, vasculature, endoneural and perineural cells, cells of the immune system, and some blood. (**a**) Schematic showing the investigated regions of the sensory-motor system. (**b**) The regions of interest shown on the image depicting the *m/z* 865 ion distribution. Scale bar = 500 µm. The molecular image was normalized to total ion count. (**c**) Microphotograph of the freshly isolated regions. Red asterisk = area with no tissue where control data were collected in MSI experiments

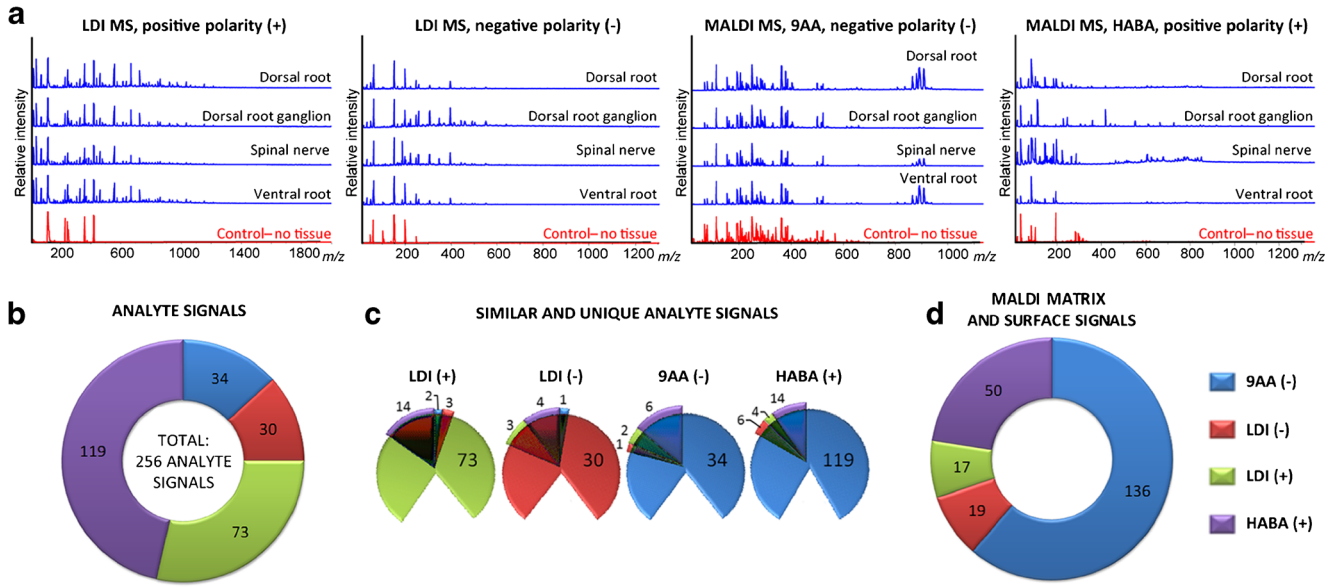

Figure 2. The combination of distinct MALDI matrices, positive and negative mode, and LDI and MALDI modes increased the number of peaks observed. (**a**) Representative mass spectra acquired during MSI of different regions of the mammalian sensory-motor neuronal network using LDI-MS and MALDI-MS. (**b**) The number of peaks observed, including the total number, and those specific for each approach. (**c**) The total number of signals observed by each approach with the number of those specific signals detected by other approaches as an overlay (solely based on *m/z*); in no case was the overlap more than 30%. (**d**) Each method detected a variety of unique background signals. The polarity of the mass spectrometer operation is shown in parenthesis

characteristic for both roots, and the compound with *m/z* 887 was observed predominantly in DRGs. Other examples of specific localization of sources of molecular signals are presented in Figure 3.

As a discovery tool, MALDI-MSI effectively highlights the putative differences in the chemical composition of different biological structures, and this guides further investigations. For example, the image of the distribution of the analyte with *m/z*

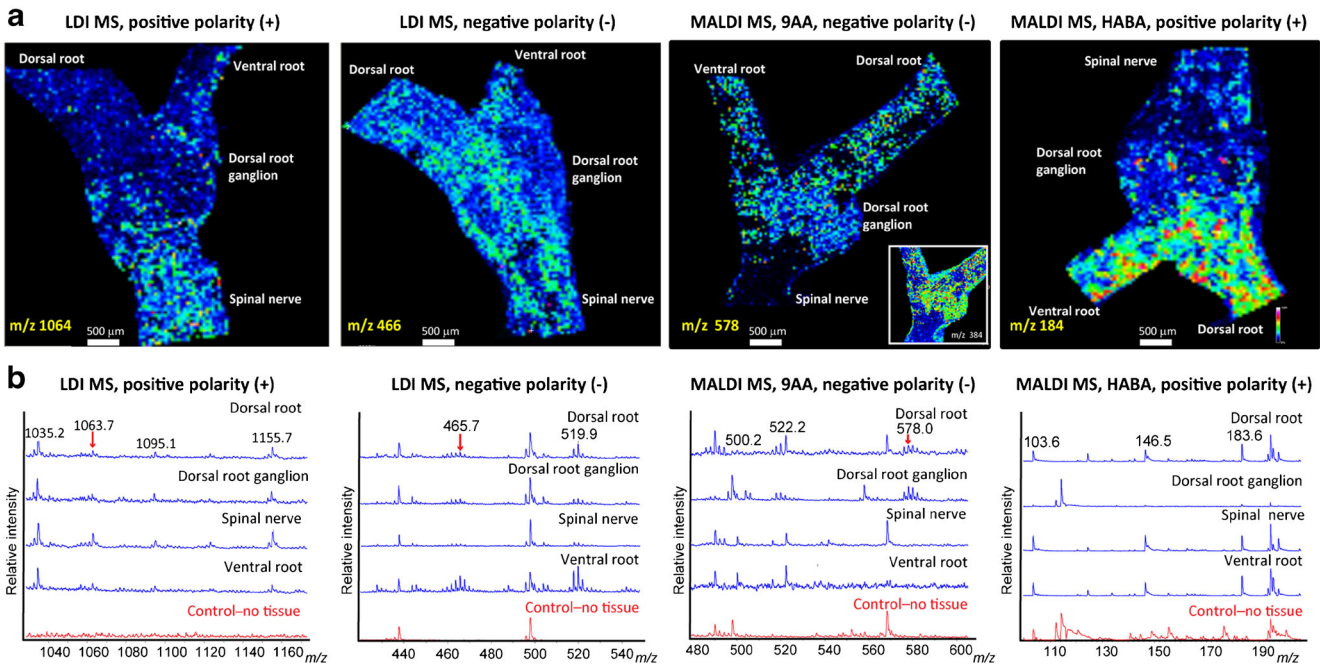

Figure 3. Putative biomarkers for different regions of the mammalian sensory-motor neuronal network are detected. (**a**) Images of different biomarker distributions in distinct regions of the mammalian sensory-motor neuronal network. (**b**) Representative mass spectra of the data pools acquired during MSI of the regions shown above. Molecular images were normalized to total ion count. The polarity of the mass spectrometer operation is shown in parenthesis

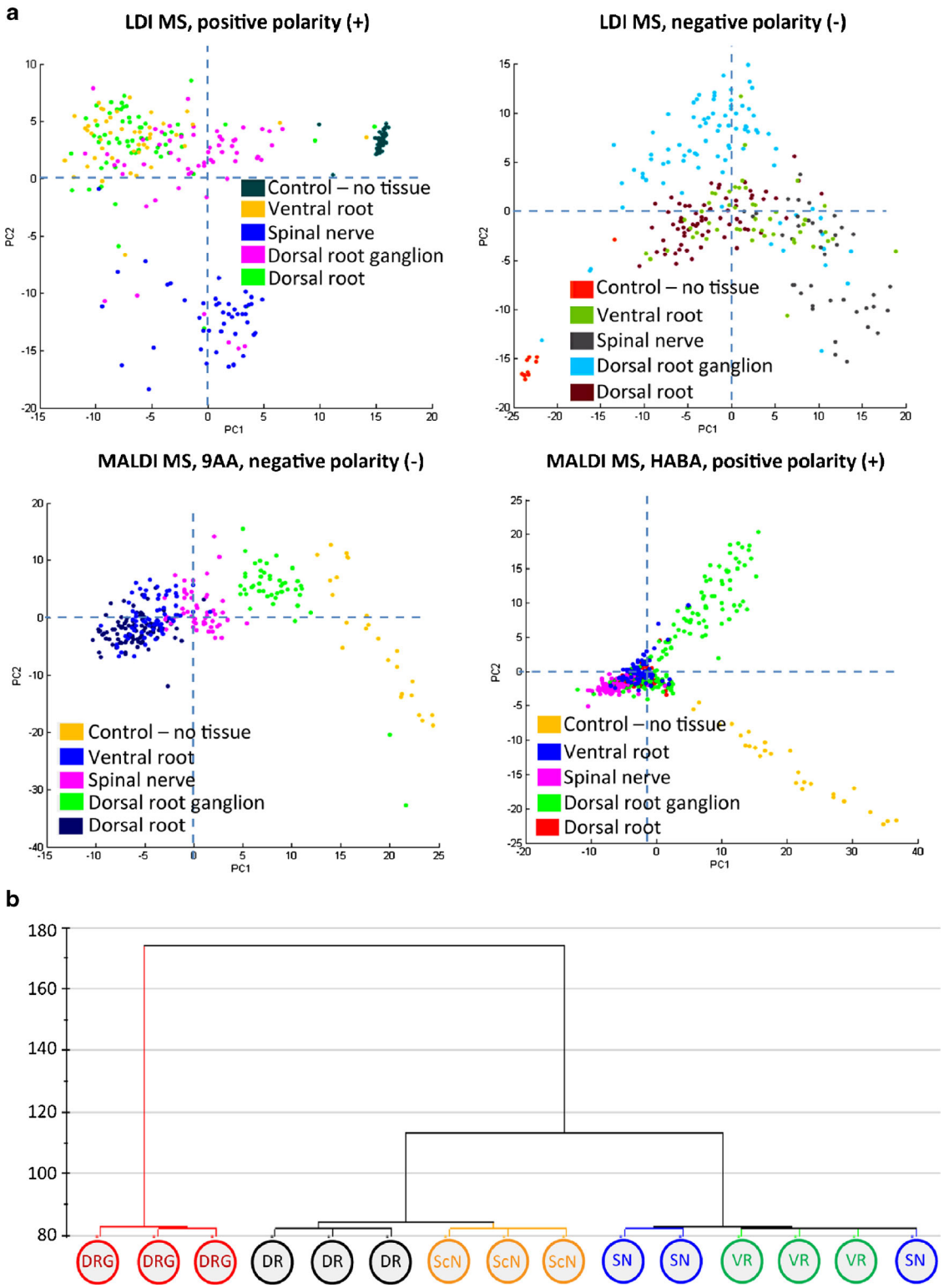

Figure 4. Results of statistical analysis of MS and GC-MS data sets acquired from different regions of the mammalian sensory-motor system. (**a**) PCA analysis of the data pools acquired during MSI revealed important differences between the functional regions. Principal component scores with each point representing a pixel in the region of interest in representative images for each analytical approach. (**b**) Cluster dendrogram illustrating the differences and clustering of mammalian sensory-motor system regions based on OPLS/O2PLS-DA of GC-MS data and model. Regions are clustered in accordance with their metabolite content and function. Data from individual measurements of the lower and upper fractions of the two-phase analyte extraction were combined for each sample. Three experiments were conducted utilizing samples from three different animals. DRG = dorsal root ganglion; DR = dorsal root; ScN = sciatic nerve; SN = spinal nerve; VR = ventral root

883 demonstrates the biochemical differences between ventral and dorsal root neurons and/or glia-related structures, and allows us to follow its contribution to the formation of the spinal nerve (Supplementary Figure S1a; ventral root component outlined by dashed line). Additionally, visual observation of the distribution of molecular signals helps to uncover potentially interesting low-intensity signals from endogenous compounds (Supplementary Figure S1b). Such signals have a low signal to noise ratio and, typically, are excluded from peak peaking by automatic mass spectra processing.

GC-MS Analysis of the Mammalian Sensory-Motor Network

Although the biochemical heterogeneity of the mammalian sensory-motor network has been highlighted in the experiments described above, known effects of analyte suppression and enhancement suggest the use of a distinct analytical approach to validate the view established here that DRGs and adjacent nerves are chemically different. We utilized the classic GC-MS approach for this task. We investigated single DRGs and small pieces of adjacent nerves as individual samples. Small amounts of material—consisting of less than 20 (DRGs) to several hundred (distal part of sciatic nerve) milligrams of wet tissue—were collected; 206 compounds were detected in all samples (Supplementary Table S3). Possibly, because of the small amount of material available, not all compounds were observed in each sample. We characterized 58 detected compounds known to be involved in carbohydrate-energy metabolism, including sugar, ascorbate, and nucleotide metabolism, and the TCA cycle. Such compounds were detected in all regions, with glucose and lactic acid present at high levels. Nitrogen metabolism is also well represented by the presence of 31 metabolites. The classic neurotransmitters gamma-aminobutyric acid, glutamic acid, and aspartic acid were among the substances detected. Lipid metabolism is described by 96 sterols, alkenes, fatty alcohols, and fatty acids and their derivatives. Predictably, endogenous cholesterol and the stabilization agent glycerol added to the samples are present at high levels in most of the samples. Vitamin E-related compounds, including alpha-tocopherol and gamma-tocopherol, were observed in some samples, as well as five different phosphates (2-aminoethylphosphate, 3-[(2,2-dimethylpropylidene)amino]propylphosphate, monomethylphosphate, pyrophosphate (4:1), and an ester of phosphoric acid, which had the highest levels among the phosphates present).

Do the Defined Regions Have Distinct Chemical Profiles?

We wanted to determine if each anatomically defined region of the studied mammalian sensory-motor system had distinct chemical profiles. Thus, we applied PCA using the MSI dataset and OPLS-DA using the GC-MS data. As highlighted in Figure 4, the MSI data are well separated into the distinct regions. In addition, the results of the OPLS-DA well match the functional and structural organization of the biological system. The OPLS-DA modeling discriminates two main groups of samples and finds important metabolic markers related to these differences (Supplementary Figure S2). The OPLS-DA model (Figure 4b) revealed good sample clustering but poor prediction ability (Q2 = –15.3%). This positive outcome of the analyses, taking into account our relatively poor GC-MS dataset with a number of analytes detected only in a subset of samples, is somewhat surprising. Predictably, our statistical analyses of the GC-MS and MSI data revealed that nerves and DRGs are the most chemically distinct (Figure 4). This is expected as the cell bodies of sensory neurons, as well as several other cell types such as satellite cells, are present only in the DRG samples. The samples also possess Schwann cells and neurites, which are most abundant in nerves. The cellular composition and chemical profiles of nerve samples are similar to each other. However, there are subtle differences between the dorsal and ventral roots according to the GC-MS data, and the spinal nerve and the rest of the nerves from the MSI data.

Intriguingly, the spinal nerve has more similarity to the dorsal root than the distal portion of the sciatic nerve collected from the rat's leg, with the latter being chemically similar to the ventral root. The observation of the longitudinal difference in spinal-sciatic nerve structure biochemistry is in good agreement with published data demonstrating longitudinal variation in nerve morphometric parameters [63–65]. The perimeter of the axon, along with other parameters, was found to be significantly greater in the proximal part of the phrenic nerve than in the distal. However, in contrast, two nerves located in the leg, the sural nerve (a sensory branch of the sciatic nerve) and the saphenous nerve, did not demonstrate morphometric differences between their proximal and distal parts [66–68]. The close location of the DRG and spinal cord to the analyzed spinal nerve may be responsible for the biochemical differences we detected.

Conclusions

A high degree of chemical heterogeneity was observed in physically connected and adjacent regions of the mammalian sensory-motor system consisting of DRGs, the sciatic nerve, and ventral and dorsal roots. The chemical heterogeneity matches the functional and structural differences that the regions exhibit. The combination of several spatially-resolved MS approaches increased the information content and enabled these differences to be highlighted. We are now working to correlate the observed differences to the function of these structures, and to relate them to the specific structures and cells founds within them. A better understanding of the chemical composition of DRGs and adjacent nerves may help us to understand mechanisms of pain and develop advanced therapies for managing pain and to aid nerve regeneration.

Acknowledgments

The authors acknowledge support for this work by the National Institute of Mental Health under Award no. R21 MH100704A

and the National Institute on Drug Abuse under Award no. P30 DA018310, and the National Science Foundation Division of Chemistry under grant CHE-11-11705 (with co-funding from the Division of Biological Infrastructure). The content is solely the responsibility of the authors and does not necessarily represent the official views of the funding agencies. Technical support by Xiying Wang is gratefully acknowledged.

References

1. McDonnell, L.A., Heeren, R.M.: Imaging mass spectrometry. Mass Spectrom. Rev. **26**, 606–643 (2007)
2. Rubakhin, S.S., Sweedler, J.V.: A mass spectrometry primer for mass spectrometry imaging. Methods Mol. Biol. **656**, 21–49 (2010)
3. Rubakhin, S.S., Hatcher, N.G., Monroe, E.B., Heien, M.L., Sweedler, J.V.: Mass spectrometric imaging of the nervous system. Curr. Pharm. Des. **13**, 3325–3334 (2007)
4. Chaurand, P., Sanders, M.E., Jensen, R.A., Caprioli, R.M.: Proteomics in diagnostic pathology: profiling and imaging proteins directly in tissue sections. Am. J. Pathol. **165**, 1057–1068 (2004)
5. Gessel, M.M., Norris, J.L., Caprioli, R.M.: MALDI imaging mass spectrometry: spatial molecular analysis to enable a new age of discovery. J. Proteome **107**, 71–82 (2014)
6. Wu, C., Dill, A.L., Eberlin, L.S., Cooks, R.G., Ifa, D.R.: Mass spectrometry imaging under ambient conditions. Mass Spectrom. Rev. **32**, 218–243 (2013)
7. Setou, M., Kurabe, N.: Mass microscopy: high-resolution imaging mass spectrometry. J. Electron Microsc. (Tokyo) **60**, 47–56 (2011)
8. Cornett, D.S., Frappier, S.L., Caprioli, R.M.: MALDI-FTICR imaging mass spectrometry of drugs and metabolites in tissue. Anal. Chem. **80**, 5648–5653 (2008)
9. Petyuk, V.A., Qian, W.J., Chin, M.H., Wang, H., Livesay, E.A., Monroe, M.E., Adkins, J.N., Jaitly, N., Anderson, D.J., Camp II, D.G., Smith, D.J., Smith, R.D.: Spatial mapping of protein abundances in the mouse brain by voxelation integrated with high-throughput liquid chromatography-mass spectrometry. Genome Res. **17**, 328–336 (2007)
10. Stoeckli, M., Chaurand, P., Hallahan, D.E., Caprioli, R.M.: Imaging mass spectrometry: a new technology for the analysis of protein expression in mammalian tissues. Nat. Med. **7**, 493–496 (2001)
11. McLean, J.A., Fenn, L.S., Enders, J.R.: Structurally selective imaging mass spectrometry by imaging ion mobility-mass spectrometry. Methods Mol. Biol. **656**, 363–383 (2010)
12. Woods, A.S., Jackson, S.N.: The application and potential of ion mobility mass spectrometry in imaging MS with a focus on lipids. Methods Mol. Biol. **656**, 99–111 (2010)
13. Stauber, J., MacAleese, L., Franck, J., Claude, E., Snel, M., Kaletas, B.K., Wiel, I.M., Wisztorski, M., Fournier, I., Heeren, R.M.: On-tissue protein identification and imaging by MALDI-ion mobility mass spectrometry. J. Am. Soc. Mass Spectrom. **21**, 338–347 (2010)
14. McLean, J.A., Ridenour, W.B., Caprioli, R.M.: Profiling and imaging of tissues by imaging ion mobility-mass spectrometry. J. Mass Spectrom. **42**, 1099–1105 (2007)
15. Manicke, N.E., Dill, A.L., Ifa, D.R., Cooks, R.G.: High-resolution tissue imaging on an orbitrap mass spectrometer by desorption electrospray ionization mass spectrometry. J. Mass Spectrom. **45**, 223–226 (2010)
16. Schober, Y., Guenther, S., Spengler, B., Rompp, A.: Single cell matrix-assisted laser desorption/ionization mass spectrometry imaging. Anal. Chem. **84**, 6293–6297 (2012)
17. Chen, B., Lietz, C.B., Li, L.: In situ characterization of proteins using laserspray ionization on a high-performance MALDI-LTQ-Orbitrap mass spectrometer. J. Am. Soc. Mass Spectrom. **25**, 2177–2180 (2014)
18. Tomlinson, L., Fuchser, J., Futterer, A., Baumert, M., Hassall, D.G., West, A., Marshall, P.S.: Using a single, high mass resolution mass spectrometry platform to investigate ion suppression effects observed during tissue imaging. Rapid Commun. Mass Spectrom. **28**, 995–1003 (2014)
19. Todd, P.J., Schaaff, T.G., Chaurand, P., Caprioli, R.M.: Organic ion imaging of biological tissue with secondary ion mass spectrometry and matrix-assisted laser desorption/ionization. J. Mass Spectrom. **36**, 355–369 (2001)
20. Vickerman, J.C.: Molecular imaging and depth profiling by mass spectrometry—SIMS, MALDI or DESI? Analyst **136**, 2199–2217 (2011)
21. Touboul, D., Roy, S., Germain, D.P., Chaminade, P., Brunelle, A., Laprevote, O.: MALDI-TOF and cluster-TOF-SIMS imaging of Fabry disease biomarkers. Int. J. Mass Spectrom. **260**, 158–165 (2007)
22. Monroe, E.B., Annangudi, S.P., Hatcher, N.G., Gutstein, H.B., Rubakhin, S.S., Sweedler, J.V.: SIMS and MALDI MS imaging of the spinal cord. Proteomics **8**, 3746–3754 (2008)
23. National Institute of Standards and Technology. Available at: http://maldi.nist.gov. Accessed 26 Jan (2015)
24. Caprioli, R.M., Farmer, T.B., Gile, J.: Molecular imaging of biological samples: localization of peptides and proteins using MALDI-TOF MS. Anal. Chem. **69**, 4751–4760 (1997)
25. Zimmerman, T.A., Rubakhin, S.S., Sweedler, J.V.: Mass spectrometry imaging using the stretched sample approach. Methods Mol. Biol. **656**, 465–479 (2010)
26. Rompp, A., Guenther, S., Schober, Y., Schulz, O., Takats, Z., Kummer, W., Spengler, B.: Histology by mass spectrometry: label-free tissue characterization obtained from high-accuracy bioanalytical imaging. Angew. Chem. **49**, 3834–3838 (2010)
27. Becker, J.S., Kumtabtim, U., Wu, B., Steinacker, P., Otto, M., Matusch, A.: Mass spectrometry imaging (MSI) of metals in mouse spinal cord by laser ablation ICP-MS. Metallomics **4**, 284–288 (2012)
28. Girod, M., Shi, Y., Cheng, J.X., Cooks, R.G.: Mapping lipid alterations in traumatically injured rat spinal cord by desorption electrospray ionization imaging mass spectrometry. Anal. Chem. **83**, 207–215 (2011)
29. Hanrieder, J., Ekegren, T., Andersson, M., Bergquist, J.: MALDI imaging of post-mortem human spinal cord in amyotrophic lateral sclerosis. J. Neurochem. **124**, 695–707 (2013)
30. Hanrieder, J., Ewing, A.G.: Spatial elucidation of spinal cord lipid- and metabolite- regulations in amyotrophic lateral sclerosis. Sci. Rep. **4**, 5266 (2014)
31. Tucker, K.R., Serebryannyy, L.A., Zimmerman, T.A., Rubakhin, S.S., Sweedler, J.V.: The modified-bead stretched sample method: development and application to MALDI-MS imaging of protein localization in the spinal cord. Chem. Sci. **2**, 785–795 (2011)
32. Ye, H., Hui, L.M., Kellersberger, K., Li, L.J.: Mapping of neuropeptides in the crustacean stomatogastric nervous system by imaging mass spectrometry. J. Am. Soc. Mass Spectrom. **24**, 134–147 (2013)
33. Li, L., Moroz, T.P., Garden, R.W., Floyd, P.D., Weiss, K.R., Sweedler, J.V.: Mass spectrometric survey of interganglionically transported peptides in Aplysia. Peptides **19**, 1425–1433 (1998)
34. Cheng, H., Sun, G., Yang, K., Gross, R.W., Han, X.L.: Selective desorption/ionization of sulfatides by MALDI-MS facilitated using 9-aminoacridine as matrix. J. Lipid Res. **51**, 1599–1609 (2010)
35. Anderson, D.M.G., Mills, D., Spraggins, J., Lambert, W.S., Calkins, D.J., Schey, K.L.: High-resolution matrix- assisted laser desorption ionization-imaging mass spectrometry of lipids in rodent optic nerve tissue. Mol. Vis. **19**, 581–592 (2013)
36. Patti, G.J., Yanes, O., Shriver, L.P., Courade, J.P., Tautenhahn, R., Manchester, M., Siuzdak, G.: Metabolomics implicates altered sphingolipids in chronic pain of neuropathic origin. Nat. Chem. Biol. **8**, 232–234 (2012)
37. Katano, T., Mabuchi, T., Okuda-Ashitaka, E., Inagaki, N., Kinumi, T., Ito, S.: Proteomic identification of a novel isoform of collapsin response mediator protein-2 in spinal nerves peripheral to dorsal root ganglia. Proteomics **6**, 6085–6094 (2006)
38. Muir, W.W., Woolf, C.J.: Mechanisms of pain and their therapeutic implications. J. Am. Vet. Med. Assoc. **219**, 1346–1356 (2001)
39. Scholz, J., Woolf, C.J.: Can we conquer pain? Nat. Neurosci. **5**, 1062–1067 (2002)
40. Woolf, C.J.: Pain: moving from symptom control toward mechanism-specific pharmacologic management. Ann. Intern. Med. **140**, 441–451 (2004)
41. Devor, M.: Unexplained peculiarities of the dorsal root ganglion. Pain. Suppl **6**, S27–S35 (1999)
42. Ding, H., Goldberg, M.M., Raymer, J.H., Holmes, J., Stanko, J., Chaney, S.G.: Determination of platinum in rat dorsal root ganglion using ICP-MS. Biol. Trace Elem. Res. **67**, 1–11 (1999)
43. Cheng, H., Jiang, X., Han, X.: Alterations in lipid homeostasis of mouse dorsal root ganglia induced by apolipoprotein E deficiency: a shotgun lipidomics study. J. Neurochem. **101**, 57–76 (2007)
44. Wong, A., Sagar, D.R., Ortori, C.A., Kendall, D.A., Chapman, V., Barrett, D.A.: Simultaneous tissue profiling of eicosanoid and endocannabinoid lipid families in a rat model of osteoarthritis. J. Lipid Res. **55**, 1902–1913 (2014)

45. Rimmerman, N., Hughes, H.V., Bradshaw, H.B., Pazos, M.X., Mackie, K., Prieto, A.L., Walker, J.M.: Compartmentalization of endocannabinoids into lipid rafts in a dorsal root ganglion cell line. Br. J. Pharmacol. **153**, 380–389 (2008)
46. Mar, F.M., Simoes, A.R., Leite, S., Morgado, M.M., Santos, T.E., Rodrigo, I.S., Teixeira, C.A., Misgeld, T., Sousa, M.M.: CNS axons globally increase axonal transport after peripheral conditioning. J. Neurosci. **34**, 5965–5970 (2014)
47. Zhang, X.J., Leung, F.P., Hsiao, W.W.L., Tan, S., Li, S., Xu, H.X., Sung, J.J.Y., Bian, Z.X.: Proteome profiling of spinal cord and dorsal root ganglia in rats with trinitrobenzene sulfonic acid-induced colitis. World J. Gastroenterol. **18**, 2914–2928 (2012)
48. Komori, N., Takemori, N., Kim, H.K., Singh, A., Hwang, S.H., Foreman, R.D., Chung, K., Chung, J.M., Matsumoto, H.: Proteomics study of neuropathic and nonneuropathic dorsal root ganglia: altered protein regulation following segmental spinal nerve ligation injury. Physiol. Genomics **29**, 215–230 (2007)
49. Riedl, M.S., Braun, P.D., Kitto, K.F., Roiko, S.A., Anderson, L.B., Honda, C.N., Fairbanks, C.A., Vulchanova, L.: Proteomic analysis uncovers novel actions of the neurosecretory protein VGF in nociceptive processing. J. Neurosci. **29**, 13377–13388 (2009)
50. Benabdellah, F., Touboul, D., Brunelle, A., Laprevote, O.: In situ primary metabolites localization on a rat brain section by chemical mass spectrometry imaging. Anal. Chem. **81**, 5557–5560 (2009)
51. Le Belle, J.E., Harris, N.G., Williams, S.R., Bhakoo, K.K.: A comparison of cell and tissue extraction techniques using high-resolution 1H-NMR spectroscopy. NMR Biomed. **15**, 37–44 (2002)
52. Roessner, U., Wagner, C., Kopka, J., Trethewey, R.N., Willmitzer, L.: Simultaneous analysis of metabolites in potato tuber by gas chromatography-mass spectrometry. Plant J. **23**, 131–142 (2000)
53. National Institute of Standards and Technology. Available at: http://www.amdis.net/index.html. Accessed 31 Jan (2015)
54. Wiley Registry of Mass Spectral Data. Available at: http://www.sisweb.com/software/ms/wiley.htm. Accessed 31 Jan (2015)
55. Westerhuis, J., Hoefsloot, H.J., Smit, S., Vis, D., Smilde, A., van Velzen, E.J., van Duijnhoven, J.M., van Dorsten, F.: Assessment of PLSDA cross validation. Metabolomics **4**, 81–89 (2008)
56. Trygg, J., Holmes, E., Lundstedt, T.: Chemometrics in metabonomics. J. Proteome Res. **6**, 469–479 (2007)
57. Smit, S., van Breemen, M.J., Hoefsloot, H.C., Smilde, A.K., Aerts, J.M., de Koster, C.G.: Assessing the statistical validity of proteomics based biomarkers. Anal. Chim. Acta **592**, 210–217 (2007)
58. Wiklund, S., Johansson, E., Sjostrom, L., Mellerowicz, E.J., Edlund, U., Shockcor, J.P., Gottfries, J., Moritz, T., Trygg, J.: Visualization of GC/TOF-MS-based metabolomics data for identification of biochemically interesting compounds using OPLS class models. Anal. Chem. **80**, 115–122 (2008)
59. Bro, R., Smilde, A.K.: Centering and scaling in component analysis. J. Chemometr. **17**, 16–33 (2003)
60. van den Berg, R.A., Hoefsloot, H.C., Westerhuis, J.A., Smilde, A.K., van der Werf, M.J.: Centering, scaling, and transformations: improving the biological information content of metabolomics data. BMC Genomics **7**, 142 (2006)
61. Storey, J.D.: A direct approach to false discovery rates. J. R. Stat. Soc. Ser. (Stat. Methodol.) **64**, 479–498 (2002)
62. Gode, D., Volmer, D.A.: Lipid imaging by mass spectrometry—a review. Analyst **138**, 1289–1315 (2013)
63. Fraher, J.P.: Myelin-axon relationships in the rat phrenic nerve: longitudinal variation and lateral asymmetry. J. Comp. Neurol. **323**, 551–557 (1992)
64. Lubinska, L., Waryszewska, J.: Fibre population of the phrenic nerve of rat: changes of myelinated fibre dimensions along the nerve and characteristics of axonal branchings. Acta Neurobiol. Exp. (Wars) **34**, 525–541 (1974)
65. Rodrigues, A.R., Ferreira, R.S., Salgado, H.C., Fazan, V.P.: Morphometric analysis of the phrenic nerve in male and female Wistar-Kyoto (WKY) and spontaneously hypertensive rats (SHR). Braz. J. Med. Biol. Res. **44**, 583–591 (2011)
66. Jeronimo, A., Jeronimo, C.A., Rodrigues Filho, O.A., Sanada, L.S., Fazan, V.P.: A morphometric study on the longitudinal and lateral symmetry of the sural nerve in mature and aging female rats. Brain Res. **1222**, 51–60 (2008)
67. Jeronimo, A., Jeronimo, C.A., Rodrigues Filho, O.A., Sanada, L.S., Fazan, V.P.: Microscopic anatomy of the sural nerve in the postnatal developing rat: a longitudinal and lateral symmetry study. J. Anat. **206**, 93–99 (2005)
68. Campos, S.A., Sanada, L.S., Sato, K.L., Fazan, V.P.: Morphometry of saphenous nerve in young rats. J. Neurosci. Methods **168**, 8–14 (2008)